Progress In Electromagnetics Research C, Vol. 41, 137–150, 2013

COMPACT MICROSTRIP DUAL-MODE DUAL-BAND BAND-PASS FILTERS USING STUBS LOADED COUPLED LINE

Jin Xu* **and Wen Wu**

Ministerial Key Laboratory of JGMT, Nanjing University of Science and Technology, Nanjing 210094, China

Abstract—This paper presents two novel dual-mode dual-band bandpass filters (BPFs) by using stubs loaded coupled line. The analytical equations of their transmission poles and transmission zeros are given by the classical even-/odd-mode method. Design rules for two dual-band BPFs are also given, which show the easily tuned passband frequency locations and in-band performance. As examples, two dual-mode dual-band BPFs, dual-band filter A with central frequencies (CFs) at 3.5/6.8 GHz and −3 dB fractional bandwidth (FBW) of 14%/10%, while dual-band filter B with CFs at 2.4/6.8 GHz and −3 dB FBW of 43%/16% are designed, fabricated and measured. Good agreement can be observed between the simulations and measurements. These two filters exhibit simple design procedures, simple physical topology, low insertion losses, good return losses, high isolation and compact sizes.

1. INTRODUCTION

As a key component in modern dual-service communication system, dual-band bandpass filter (BPF) with compact size, low in-band insertion loss and high isolation is in great demand, so as to handle dual-service in a single radio-frequency (RF) module.

To meet the above requirements, various dual-band BPFs have been reported. The most popular dual-band BPF design method is to use the fundamental resonance frequency of net-type resonator [1] or stepped-impedance resonator (SIR) [2] forming the first passband while to use their spurious frequencies building up the second passband. Combing two different sizes of resonators together is another effective

Received 22 May 2013, Accepted 22 June 2013, Scheduled 27 June 2013
* Corresponding author: Jin Xu (xujin2njust@126.com).

way to design dual-band BPF [3]. The resonators with longer electrical length are used to design the lower passband, while the resonators with shorter electrical length are used to design the upper passband. To achieve compact size, both meander technology and the fractal geometry are utilized in filter design [3]. The merit of above two methods is its easily tuned central frequencies (CFs) of two passbands. The multi-mode resonator is also often used to develop the compact dual-band BPF [4]. Since the resonance modes of multi-mode resonator sometimes cannot be controlled separately, this type of dual-band filter may not be able to get the desired CFs of two passbands. There have been some another methods to exploit dual-band BPFs [5, 6]. In [5], a hybrid transmission line and coupled line unit cell with dual-band performance is reported. In [6], two dual-mode dual-band BPFs are proposed by using a frequencyselecting coupling structure with coupled lines at its input/output ports. So far, some advanced fabrication techniques have been used in dual-band filter development [7–10]. The techniques of integrated passive device (IPD) [7], multilayer low-temperature co-fired ceramic (LTCC) [8, 9], and multilayer organic substrate [10] are employed. Compared with the standard printed-circuit-board (PCB) technique, the fabrication cost of these four filters are relatively high. In addition, their electrical performances and circuit sizes are also not good enough, i.e., large insertion loss [8, 10] and large circuit size [9, 10].

All the above dual-band BPFs reported in [1–10] have a narrow bandwidth in both two passbands or one of its passbands, which cannot meet the modern dual high data-rate communication requirement. Recently, several dual-wideband BPFs have been reported [11–19]. In [11], the dual-wideband BPFs using frequency mapping and SIRs are proposed, with the drawback of complex design procedures and large circuit sizes. In [12–14], dual-band BPFs are designed by using SIRs. However, these three dual-wideband BPFs suffer from many disadvantages, i.e., poor passband selectivity [12, 13], large circuit size [13] and complex physical topology [14]. Opposite hook-shaped resonator [15] and comb-loaded resonator [16] are proposed to develop dual-wideband BPFs. These two dual-wideband BPFs achieve compact sizes and high passband selectivity in both passbands, but also suffer from poor band-to-band isolation [15] or large insertion loss [16]. The dual-wideband BPFs by using coupled-line in [17] and transversal-interaction concept in [18] exhibit good in-band performance and wide stopband, but also suffer from large circuit sizes. In [19], two dual-mode dual-band BPFs are reported by using novel quadruple-mode resonator. These two filters have the merits of sharp skirts, high isolation, low in-band insertion loss and compact size, but the etched ground plane is used, which increases the installation complexity. Thus, it is still significant for RF designers to exploit compact dual-wideband BPF with high performance.

This paper presents two novel dual-mode dual-band BPF structures, i.e., dual-band filter A and dual-band filter B. Dual-band filter A have two narrow passbands, and dual-band filter B exhibits two wide passbands. Design rules for two dual-band BPFs are also given, which show their simple design procedure. As examples, two dual-mode dual-band BPFs, dual-band filter A with CFs at 3.5/6.8 GHz and −3 dB fractional bandwidth (FBW) of 14%/10%, while dual-band filter B with CFs at 2.4/6.8 GHz and −3 dB FBW of 43%/16% are designed, fabricated and measured. Two filters are designed on the substrate ARlon DiClad 880 ($h = 0.508$ mm, $\varepsilon_{re} = 2.2$ and $\tan\delta = 0.0009$). The designed two filters exhibit simple physical topology, low insertion losses, good return losses, high isolation and compact sizes. Detailed design procedures as well as simulated and measured results are discussed in the following sections.

2. CHARACTERISTICS OF PROPOSED DUAL-BAND BPF STRUCTURES

Figures 1(a) and (b) give the transmission line model of proposed dual-band filter A and B, respectively. Dual-band filter A consists of two quarter-wavelength impedance Z_{a1} sections ($\theta_{a1} = \pi/2$ at the designing frequency f_{a0}), one quarter-wavelength coupled line section ($\theta_{ac} = \pi/2$ at f_{a0}) and two shorted half-wavelength impedance Z_{a2} sections ($\theta_{a2} = \pi$ at f_{a0}) loaded on the two ends of coupled line section. Dual-band filter B consists of two quarter-wavelength impedance Z_{b1} sections ($\theta_{b1} = \pi/2$ at the designing frequency f_{b0}), one quarter-wavelength coupled line ($\theta_{bc} = \pi/2$ at f_{b0}) and two open quarter-wavelength impedance Z_{b2} sections ($\theta_{b2} = \pi/2$ at f_{a0}) loaded on the two ends of coupled line section. Since the difference between two

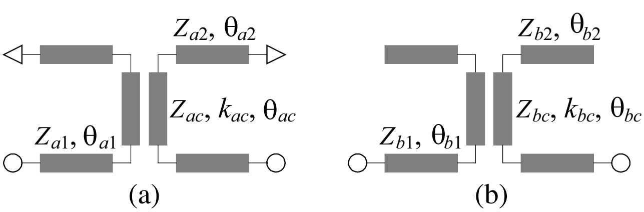

Figure 1. (a) Proposed dual-mode dual-band filter A. (b) Proposed dual-mode dual-band filter B.

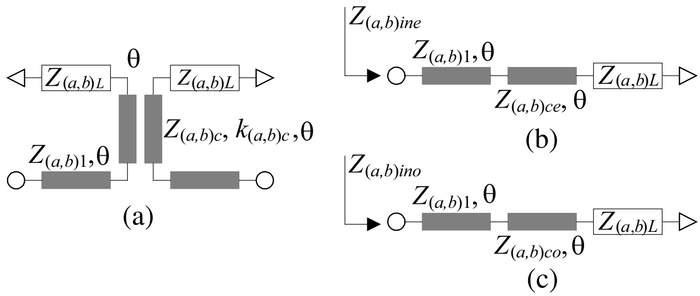

Figure 2. (a) General model of dual-mode dual-band filters A and B. (b) Even-mode equivalent circuit. (c) Odd-mode equivalent circuit.

dual-band BPF structures is the stubs loaded on the coupled line section, a general model as shown in Figure 2(a) is given to represent two structures shown in Figure 1, where $\theta = \pi/2$ at f_{a0} or f_{b0}, $Z_{aL} = jZ_{a2}\tan(2\theta)$, $Z_{bL} = -jZ_{b2}\cot\theta$, the subscripts a and b denote the dual-band filters A and B, respectively. Due to the symmetrical configuration, Figures 2(b) and (c) give the even-/odd-mode equivalent circuits, where $Z_{(a,b)ce} = Z_{(a,b)c}[(1+k_{(a,b)c})/(1-k_{(a,b)c})]^{1/2}$ and $Z_{(a,b)co} = Z_{(a,b)c}[(1-k_{(a,b)c})/(1+k_{(a,b)c})]^{1/2}$. The subscripts e and o denote even- and odd- modes, respectively. Subsequently, the one port even-/odd-mode input impedances can be derived as follows:

$$Z_{(a,b)in(e,o)} = Z_{(a,b)1}\frac{\begin{array}{c}Z_{(a,b)c(e,o)}(Z_{(a,b)L}+jZ_{(a,b)c(e,o)}\tan\theta)\\ +jZ_{(a,b)1}\tan\theta(Z_{(a,b)c(e,o)}+jZ_{(a,b)L}\tan\theta)\end{array}}{\begin{array}{c}Z_{(a,b)1}(Z_{(a,b)c(e,o)}+jZ_{(a,b)L}\tan\theta)\\ +jZ_{(a,b)c(e,o)}\tan\theta(Z_{(a,b)L}+jZ_{(a,b)c(e,o)}\tan\theta)\end{array}} \tag{1}$$

For the symmetrical and reciprocal network, its frequency response can be calculated by the following Equation [20].

$$S_{11(a,b)} = S_{22(a,b)} = \frac{Z_{(a,b)ine}Z_{(a,b)ino} - Z_0^2}{(Z_{(a,b)ine}+Z_0)(Z_{(a,b)ino}+Z_0)} \tag{2a}$$

$$S_{21(a,b)} = S_{12(a,b)} = \frac{Z_0(Z_{(a,b)ine} - Z_{(a,b)ino})}{(Z_{(a,b)ine}+Z_0)(Z_{(a,b)ino}+Z_0)} \tag{2b}$$

The even-/odd-mode resonances occur when $Z_{(a,b)ine} = \infty$ and $Z_{(a,b)ino} = \infty$, respectively. The transmission zeros (TZs) of the filter fulfill the condition $|S_{21(a,b)}| = 0$. According to these two conditions, the transmission poles (TPs) and TZs of proposed dual-band filter A and B can be derived and discussed in the following texts.

2.1. TPs and TZs of Dual-band Filter A

From Equation (1), the even-/odd-mode TPs of dual-band filter A are determined by the following Equation:

$$A_{(e,o)}\tan^4\left(\frac{\pi f_{ap(e,o)}}{2f_{a0}}\right)+B_{(e,o)}\tan^2\left(\frac{\pi f_{ap(e,o)}}{2f_{a0}}\right)+C_{(e,o)}=0 \tag{3}$$

where $f_{ap(e,o)}$ denotes the even-/odd-mode TPs, the coefficients $A_{(e,o)} = Z^2_{ac(e,o)}$, $B_{(e,o)} = -(Z_{a1}Z_{ac(e,o)} + 2Z_{a1}Z_{a2} + 2Z_{a2}Z_{ac(e,o)} + Z^2_{ac(e,o)})$, and $C_{(e,o)} = Z_{a1}Z_{ac(e,o)}$. It is clearly seen that $A_{(e,o)} > 0$, $B_{(e,o)} < 0$ and $C_{(e,o)} > 0$ are always built. For the practical designing parameters, $B^2_{(e,o)} - 4A_{(e,o)}C_{(e,o)} > 0$. Thus, the dual-band filter A has four even-mode TPs and four odd-mode TPs within $[0,\ 2f_{a0}]$, which can be given as follows:

$$f_{ap(e,o)1}=\frac{2f_{a0}}{\pi}\arctan\sqrt{\frac{-B_{(e,o)}+\sqrt{B^2_{(e,o)}-4A_{(e,o)}C_{(e,o)}}}{2A_{(e,o)}}} \tag{4a}$$

$$f_{ap(e,o)2}=\frac{2f_{a0}}{\pi}\left[\pi-\arctan\sqrt{\frac{-B_{(e,o)}+\sqrt{B^2_{(e,o)}-4A_{(e,o)}C_{(e,o)}}}{2A_{(e,o)}}}\right] \tag{4b}$$

$$f_{ap(e,o)3}=\frac{2f_{a0}}{\pi}\arctan\sqrt{\frac{-B_{(e,o)}-\sqrt{B^2_{(e,o)}-4A_{(e,o)}C_{(e,o)}}}{2A_{(e,o)}}} \tag{4c}$$

$$f_{ap(e,o)4}=\frac{2f_{a0}}{\pi}\left[\pi-\arctan\sqrt{\frac{-B_{(e,o)}-\sqrt{B^2_{(e,o)}-4A_{(e,o)}C_{(e,o)}}}{2A_{(e,o)}}}\right] \tag{4d}$$

When $\theta = 0$, $\pi/2$ or π, $Z_{aine} = Z_{aino}$ can be fulfilled. Thus, the proposed dual-band filter A has three fixed TZs at 0, f_{a0} and $2f_{a0}$ with the frequency range $[0,\ 2f_{a0}]$. From Equation (1), the TZs of proposed dual-band filter A can be also given by

$$A_z\tan^4\left(\frac{\pi f_{az}}{2f_{a0}}\right)+B_z\tan^2\left(\frac{\pi f_{az}}{2f_{a0}}\right)+C_z=0 \tag{5}$$

where f_{az} denotes the TZs, the coefficients $A_z = 2Z_{a2}(Z_{ace} + Z_{aco}) + Z_{ace}Z_{aco}$, $B_z = -[4Z^2_{a2} + 2Z_{a2}(Z_{ace} + Z_{aco}) + 2Z_{ace}Z_{aco}]$, and $C_z = Z_{ace}Z_{aco}$. It is clearly seen that $A_z > 0$, $B_z < 0$ and $C_z > 0$ can be always built. For the practical designing parameters, $B^2_z - 4A_zC_z > 0$.

As a result, the TZs of dual-band filter A from Equation (5) can be given as

$$f_{az1} = \frac{2f_{a0}}{\pi} \arctan\sqrt{\frac{-B_z - \sqrt{B_z^2 - 4A_zC_z}}{2A_z}} \tag{6a}$$

$$f_{az2} = \frac{2f_{a0}}{\pi} \left(\pi - \arctan\sqrt{\frac{-B_z - \sqrt{B_z^2 - 4A_zC_z}}{2A_z}}\right) \tag{6b}$$

$$f_{az3} = \frac{2f_{a0}}{\pi} \arctan\sqrt{\frac{-B_z + \sqrt{B_z^2 - 4A_zC_z}}{2A_z}} \tag{6c}$$

$$f_{az4} = \frac{2f_{a0}}{\pi} \left(\pi - \arctan\sqrt{\frac{-B_z + \sqrt{B_z^2 - 4A_zC_z}}{2A_z}}\right) \tag{6d}$$

Therefore, Equations (4) and (6) allow one to determine all tunable TPs and TZs of dual-band filter A. These TPs and TZs repeat periodically at every frequency range $(2nf_{a0}, 2(n+1)f_{a0})$, where n is an integer. Within the frequency range $[0, 2f_{a0}]$, these TPs and TZs are symmetrical along f_{a0}. It can be found that these TPs and TZs have the relationship of $0 < f_{ape1} < f_{apo1} < f_{az1} < f_{az3} < f_{ape3} < f_{apo3} < f_{a0} < f_{apo4} < f_{ape4} < f_{az4} < f_{az2} < f_{apo2} < f_{ape2} < 2f_{a0}$. In the practical filter design, it is found interestingly that four TPs f_{ape1}, f_{apo1}, f_{ape2} and f_{apo2} would not build up the filter passband or the spurious passband. The fixed TZ at f_{a0} divides four TPs f_{ape3}, f_{apo3}, f_{ape4} and f_{apo4} into two groups, with one even-mode TP and one odd-mode TP in each group. These two dual-mode groups can be utilized to form two passbands. Theoretically, two passbands of dual-band filter A has a symmetrical frequency response along f_{a0}.

Under $Z_{a1} = 35\,\Omega$ and $k_{ac} = 0.35$, Figure 3 gives the variation of f_{ac2}/f_{ac1} and 3 dB absolute bandwidth (BW_a) of dual-band filter A versus $r_{ac} = Z_{ac}/Z_{a1}$ and $r_{a12} = Z_{a2}/Z_{a1}$, where $f_{ac1,2}$ denote the CFs of the first passband and the second passband, respectively. As r_{ac} increases, f_{ac2}/f_{ac1} increases while BW_a becomes small. As r_{a12} increases, f_{ac2}/f_{ac1} decreases while BW_a becomes large slowly. For a dual-band centered at 3.5/6.8 GHz ($f_{ac2}/f_{ac1} \approx 1.94$), $r_{ac} = 4.5$ and $r_{a12} = 3.8$ can be pre-selected. Under $r_{ac} = 4.5$ and $r_{a12} = 3.8$, Figure 4 plots the variation of $|S_{21}|$ and $|S_{11}|$ versus k_{ac} and Z_{a1}. It can be seen in Figure 4(a) that k_{ac} and Z_{a1} have minor effect on the CFs of two passbands and $f_{az1,2,3,4}$. The BW_a of two passbands becomes large as k_{ac} increases, while Z_{a1} almost has no effect on BW_a as shown in Figure 4(b). Therefore, in the dual-band filter A design process, r_{ac} and r_{a12} are tuned to achieve the desired f_{ac2}/f_{ac1} firstly, k_{ac} is

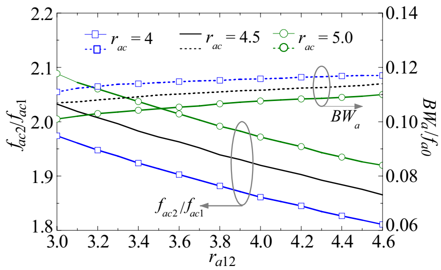

Figure 3. Variation of f_{ac2}/f_{ac1} and BW_a/f_{a0} versus r_{ac} and r_{a12}.

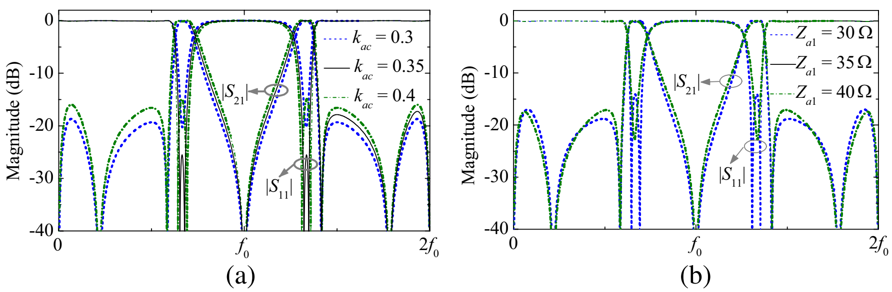

Figure 4. Variation of $|S_{21}|$ and $|S_{11}|$ versus (a) k_{ac} ($Z_{a1} = 35\,\Omega$ fixed), and (b) Z_{a1} ($k_{ac} = 0.35$ fixed).

then tuned to acquire the desired BW_a, Z_{a1} can be finally optimized to achieve a good return loss.

2.2. TPs and TZs of Dual-band Filter B

The even-/odd-mode TPs of dual-band filter B can be derived from Equation (1) as follows:

$$Z_{bc(e,o)}^2 \tan^2\left(\frac{\pi f_{bp(e,o)}}{2f_{b0}}\right) = Z_{b1}(Z_{b2} + Z_{bc(e,o)}) + Z_{b2}Z_{bc(e,o)} \tag{7}$$

Therefore, the dual-band filter B has two even-mode TPs and two odd-mode TPs within the frequency range $[0,\ 2f_{b0}]$, of which the frequency locations are given as follows:

$$f_{bp(e,o)1} = \frac{2f_{b0}}{\pi} \arctan\sqrt{\frac{Z_{b1}(Z_{b2}+Z_{bc(e,o)})+Z_{b2}Z_{bc(e,o)}}{Z_{bc(e,o)}^2}} \tag{8a}$$

$$f_{bp(e,o)2} = \frac{2f_{b0}}{\pi}\left[\pi - \arctan\sqrt{\frac{Z_{b1}(Z_{b2}+Z_{bc(e,o)})+Z_{b2}Z_{bc(e,o)}}{Z_{bc(e,o)}^2}}\right] \tag{8b}$$

Since $Z_{bine} = Z_{bino}$ can be fulfilled when $\theta = 0$, $\pi/2$ or π, the dual-band filter B also has three fixed TZs at 0, f_{b0} and $2f_{b0}$ with the frequency range $[0,\ 2f_{b0}]$. From Equation (1), the TZs of proposed dual-band filter B are given by

$$[Z_{b2}(Z_{bce}+Z_{bco})+Z_{bce}Z_{bco}]\tan^4\left(\frac{\pi f_{bz}}{2f_{b0}}\right)=Z_{b2}^2 \tag{9}$$

As a result, the dual-band filter B has two tunable TZs within the frequency range $[0,\ 2f_{b0}]$, of which the frequency locations are given as

$$f_{bz1} = \frac{2f_{b0}}{\pi}\arctan\sqrt{\frac{Z_{b2}^2}{Z_{b2}(Z_{bce}+Z_{bco})+Z_{bce}Z_{bco}}} \tag{10a}$$

$$f_{bz2} = \frac{2f_{b0}}{\pi}\left[\pi-\arctan\sqrt{\frac{Z_{b2}^2}{Z_{b2}(Z_{bce}+Z_{bco})+Z_{bce}Z_{bco}}}\right] \tag{10b}$$

Therefore, Equations (8) and (10) allow one to determine all tunable TPs and TZs of dual-band filter B. These TPs and TZs repeat periodically at every frequency range $(2nf_{b0},\ 2(n+1)f_{b0})$. Within the frequency range $[0,\ 2f_{b0}]$, these TPs and TZs are symmetrical along f_{b0}. It can be found that that these TPs and TZs have the relationship of $0 < f_{az1} < f_{ape1} < f_{apo1} < f_{b0} < f_{apo2} < f_{ape2} < f_{az2} < 2f_{b0}$. The fixed TZ at f_{b0} divides four TPs $f_{bp(e,o)(1,2)}$ into two grounds, with one even-mode TP and one odd-mode TP in each group. These two dual-mode groups can be utilized to form two passbands. Theoretically, two passbands of dual-band filter B also has a symmetrical frequency response along f_{b0}.

Under $Z_{b1} = 35\,\Omega$ and $k_{bc} = 0.45$, Figure 5 gives the variation of f_{bc2}/f_{bc1} and 3 dB absolute bandwidth (BW_b) of dual-band filter B versus $r_{bc} = Z_{bc}/Z_{b1}$ and $r_{b12} = Z_{b2}/Z_{b1}$, where $f_{bc1,2}$ denote the CFs of the first passband and the second passband, respectively. As r_{bc} increases, f_{bc2}/f_{bc1} increases while BW_b becomes small. As r_{b12} increases, both f_{bc2}/f_{bc1} and BW_b decrease. For a dual-band centered at 2.4/6.8 GHz ($f_{bc2}/f_{bc1} \approx 2.83$), $r_{bc} = 4.0$ and $r_{b12} = 3.2$ are pre-selected. Under $r_{bc} = 4.0$ and $r_{b12} = 3.2$, Figure 6 plots the variation of $|S_{21}|$ and $|S_{11}|$ versus k_{bc} and Z_{b1}. It can be seen in Figure 6(a) that k_{bc} and Z_{b1} have minor effect on the CFs of two passbands and $f_{bz1,2}$. The BW_b of two passbands becomes large as k_{bc} increases, while Z_{b1} almost has no effect on BW_b as shown in Figure 6(b). Therefore, in the dual-band filter B design process, r_{bc} and r_{b12} are tuned to achieve the desired f_{bc2}/f_{bc1} firstly, k_{bc} is then tuned to acquire the desired BW_b, Z_{b1} can be finally optimized to achieve a good return loss.

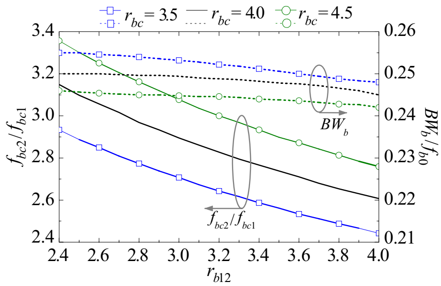

Figure 5. Variation of $|S_{21}|$ and $|S_{11}|$ versus (a) k_{ac} ($Z_{a1} = 35\,\Omega$ fixed), and (b) Z_{a1} ($k_{ac} = 0.35$ fixed).

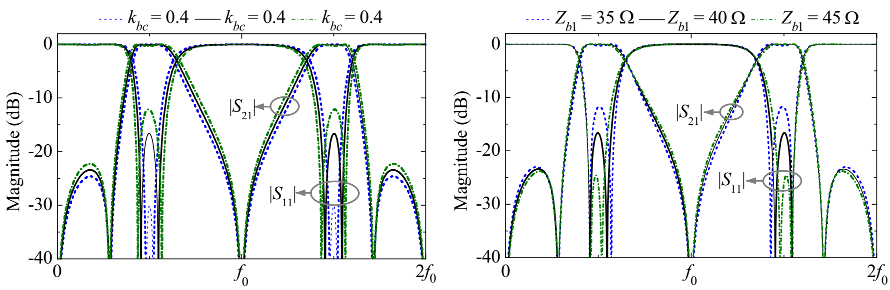

(a) (b)

Figure 6. Variation of $|S_{21}|$ and $|S_{11}|$ versus (a) k_{bc} ($Z_{b1} = 35\,\Omega$ fixed), and (b) Z_{b1} ($k_{bc} = 0.45$ fixed).

3. DUAL-BAND FILERS DESIGN AS WELL AS SIMULATED AND MEASURED RESULTS

3.1. Dual-band Filter A

According to the above discussion, the designing parameters for dual-band filter A at $f_{a0} = 5.15\,\text{GHz}$ are optimized as $Z_{1a} = 34\,\Omega$, $Z_{ca} = 148\,\Omega$, $k_{ca} = 0.34$ and $Z_{2a} = 126\,\Omega$, which corresponds to fractional bandwidth (FBWs) of 16%/8.2% and CFs at 3.5/6.8 for the WiMAX and RFID applications. The layout of fabricated dual-band filter B is given in Figure 7(a). ADS LineCalc tool are used to calculate the initial physical dimensions. The whole structure is optimized by full-wave EM-simulator HFSS, and the optimized physical dimensions are also labeled in Figure 7(a). The filter fabrication is done by using standard PCB etching process (0.08 mm minimum gap or width). The photograph of fabricated dual-band filter B is shown in Figure 7(b). Its overall circuit size is 15.96 mm × 14.5 mm (not including the feeding lines), which corresponds to $0.26\text{g}\lambda_{ga} \times 0.24\text{g}\lambda_{ga}$, where λ_{ga} represents

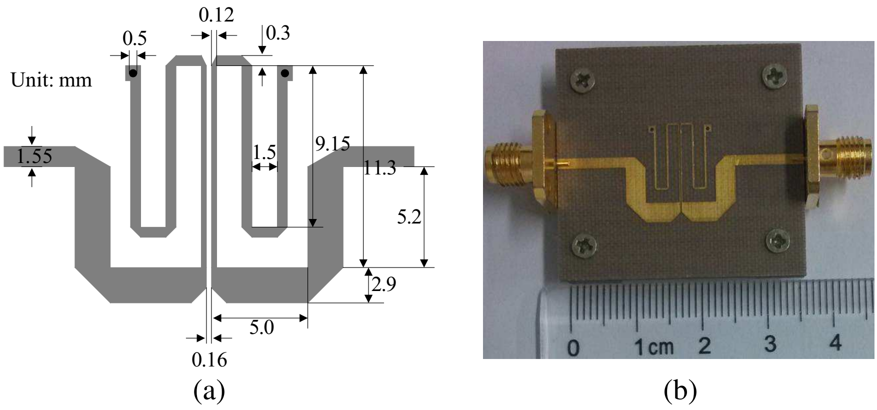

Figure 7. (a) Layout and (b) photograph of fabricated dual-band filter A.

the guided wavelength of 50 Ω microstrip line at the measured CF of its first passband on the used substrate.

Figure 8 plots the simulated and measured results of fabricated dual-band filter A. Good agreement can be observed, and some slight discrepancies are due to the fabrication error as well as SMA connectors. In addition, the analysis discussed in the above section is appropriate for microstrip line due to the unequal even-/odd-mode phase velocities, which will also cause the difference between the ideal analysis and the HFSS simulation. The measured CFs and FBWs of two passbands are 3.6/6.7 GHz and 14.4%/10.4%, respectively. The measured insertion losses (ILs) at 3.5/6.8 GHz are 0.75/0.85 dB, and the return losses are better than 20/26 dB around these two frequencies, respectively. The fabricated dual-band filter A has a 20 dB band-to-band isolation from 4.77 GHz to 5.55 GHz, 15 dB rejection lower stopband from DC to 3.27 GHz and 10 dB rejection upper stopband from 7.1 GHz to 10.34 GHz.

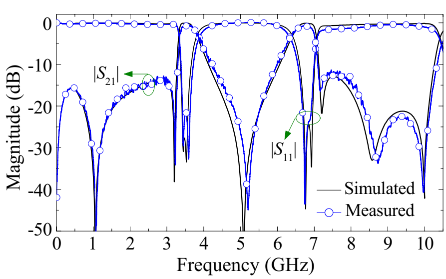

Figure 8. Simulated and measured results of the fabricated dual-band filter A.

3.2. Dual-band Filter B

According to the above discussion, the designing parameters for dual-band filter B at $f_{0b} = 4.6\,\text{GHz}$ are optimized as $Z_{1b} = 36\,\Omega$, $Z_{cb} = 146\,\Omega$, $k_{cb} = 0.43$ and $Z_{2b} = 118\,\Omega$, which corresponds to FBWs of 45.5%/16% and CFs at 2.4/6.8 for the WLAN and RFID applications. Figure 9(a) gives the layout of fabricated dual-band filter B. ADS LineCalc tool is used to calculate its initial physical dimensions. Then, the whole structure is optimized in full-wave EM-simulator HFSS and the optimized physical dimensions are also labeled in Figure 9(a). Figure 9(b) shows the photograph of fabricated dual-band filter B. Its overall circuit size is $10.92\,\text{mm} \times 15.38\,\text{mm}$ (not including the feeding lines), which corresponds to $0.12\text{g}\lambda_{gb} \times 0.17\text{g}\lambda_{gb}$, where λ_{gb} represents the guided wavelength of $50\,\Omega$ microstrip line at the measured CF of its first passband on the used substrate.

The simulated and measured results of fabricated filter B are plotted in Figure 10. Good agreement can be observed, and some

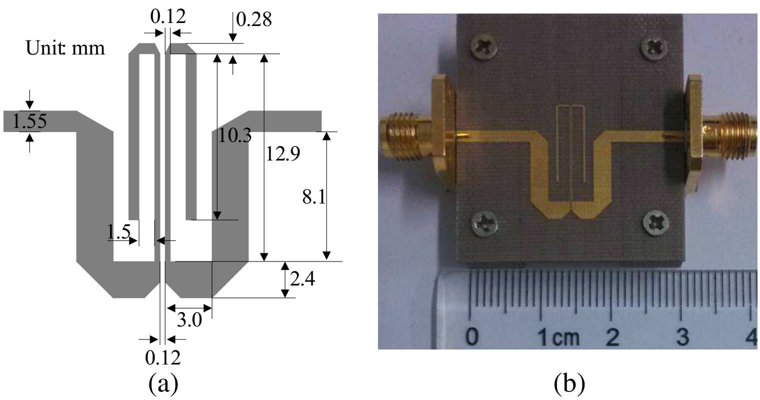

Figure 9. (a) Layout and (b) photograph of fabricated dual-band filter B.

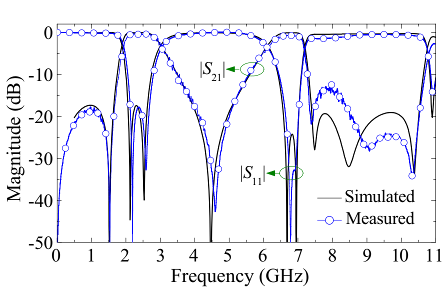

Figure 10. Simulated and measured results of the fabricated dual-band filter B.

Table 1. Performance comparison with some reported dual-band BPFs.

		CFs (GHz)/ FBW	IL at CFs (dB)	Isolation (dB)	Circuit area (λ_g^2)
[1]		1.0/4.6%, 2.0/4.8%	2.65, 2.44	> 40	0.23 × 0.17
[2]		2.4/6.3%, 5.2/3.4%	3.0, 3.0	> 30	0.48 × 0.6
[6]	Filter A	2.4/5.8%, 5.8/2.1%	1.59, 2.59	> 30	0.32 × 0.31
	Filter B	2.4/6%, 5.8/1.6%	1.6, 2.8	> 25	0.31 × 0.32
[11]	Filter 2	1.28/47.6%, 2.35/48.4%	0.5, 2	> 40	3.33 × 1.08
[13]		2.3/54%, 5.25/20%	0.8, 0.8	> 25	0.3 × 0.3
[15]		2.37/19.5%, 5.8/15.1%	0.55, 1.31	> 13	0.07 × 0.15
[16]	2nd filter	2.45/32%, 5.45/13%	1.1, 2.5	> 30	0.46 × 0.06
[18]		1.63/28.8%,2.42/22.7%	0.86, 0.97	> 15	0.69 × 0.31
[19]	Filter A	1.96/57.1%, 5.58/20.8%	0.1, 0.8	> 30	0.4 × 0.05
	Filter B	1.65/35.1%, 5.25/7.2%	0.41, 1.1	> 20	0.33 × 0.03
This work	**Dual-band filter A**	**3.6/14.4%, 6.7/10.4%**	**0.75, 0.85**	**> 20**	**0.26 × 0.24**
	Dual-band filter B	**2.48/43.2%, 6.63/16.5%**	**0.33, 0.74**	**> 20**	**0.12 × 0.17**

slight discrepancies are due to the fabrication error as well as SMA connectors. Two passbands centered at 2.48/6.63 with FBWs of 43.2%/16.5% are measured, respectively. The measured ILs at 2.4/6.8 GHz are 0.33/0.74 dB, and the return losses are better than 18/30 dB around these two frequencies, respectively. The fabricated dual-band filter B has a 20 dB band-to-band isolation from 4.13 GHz to 5.0 GHz, 18 dB rejection lower stopband from DC to 1.67 GHz and 10 dB rejection upper stopband from 7.3 GHz to 10.6 GHz.

Table 1 gives a performance comparison between this works and some reported dual-band BPFs, which shows that two proposed dual-band BPFs have the merits of high in-band performance and compact size. Moreover, the proposed dual-band BPFs have the simple design procedures and physical topologies.

4. CONCLUSION

This paper presents two novel dual-mode dual-band BPFs, i.e., dual-band filter A centered at 3.5/6.8 GHz for the application of

WiMax/RFID and dual-band filter B centered at 2.4/6.8 GHz for the application of WLAN/RFID. Dual-band filter B also has the dual-wideband property. It has been found theoretically and experimentally that the fabricated dual-band filters have the merits of low insertion losses, good return losses, high isolation and compact sizes. The fabricated filters also exhibit simple design procedures and physical topologies. Due to these merits, they are attractively used in modern communication system.

REFERENCES

1. Tseng, C.-H. and H.-Y. Shao, "A new dual-band microstrip bandpass filter using net-type resonators," *IEEE Microw. Wireless Compon. Lett.*, Vol. 20, No. 4, 196–198, 2010.
2. Ma, D., Z. Y. Xiao, L. Xiang, X. Wu, C. Huang, and X. Kou, "Compact dual-band bandpass filter using folded SIR with two stubs for WLAN," *Progress In Electromagnetics Research*, Vol. 117, 357–364, 2011.
3. Chen, C.-Y. and C.-C. Lin, "The design and fabrication of a highly compact microstrip dual-band bandpass filter," *Progress In Electromagetics Research*, Vol. 112, 299–307, 2011.
4. Chen, F.-C. and J.-M. Qiu, "Dual-band bandpass filter with controllable characteristics using stub-loaded resonators," *Progress In Electromagnetics Research Letters*, Vol. 28, 45–51, 2012.
5. Kuo, J.-T. and S.-W. Lai, "New dual-band bandpass filter with wide upper rejection band," *Progress In Electromagnetics Research*, Vol. 123, 371–384, 2012.
6. Xu, J., C. Miao, and W. Wu, "A compact and high isolation dual-mode dual-band bandpass filter with tunable transmission zeros," *Journal of Electromagnetic Waves and Applications*, Vol. 26, Nos. 17–18, 2390–2397, 2012.
7. Chen, C.-H., C.-S. Shih, T.-S. Horng, and S.-M. Wu, "Very miniature dual-band and dual-mode bandpass filter designs on an integrated passive device chip," *Progress In Electromagnetics Research*, Vol. 119, 461–476, 2011.
8. Zhou, C., Y.-X. Guo, L. Wang, and W. Wu, "Design of compact dual-band filter in multilayer LTCC with cross coupling," *Progress In Electromagnetics Research*, Vol. 135, 515–525, 2013.
9. Zhang, Q., B.-Z. Zhang, W.-Y. Yin, and L.-S. Wu, "Design of a miniaturized dual-band double-folded substrate integrated

waveguide bandpass filter with controllable bandwidths," *Progress In Electromagnetics Research*, Vol. 136, 211–223, 2013.

10. Ta, H. H. and A.-V. Pham, "Dual-band bandpass filter with wide stopband on multilayer organic substrate," *IEEE Microw. Wireless Compon. Lett.*, Vol. 23, No. 4, 193–195, 2013.
11. Liu, A.-S., T.-Y. Huang, and R.-B. Wu, "A dual-wideband filter design using frequency mapping and stepped-impedance resonators," *IEEE Trans. on Microw. Theory and Tech.*, Vol. 56, No. 12, 2921–2929, 2008.
12. Sun, X. and E. L. Tan, "A novel dual-band bandpass filter using generalized trisection stepped impedance resonator with improved out-of-band performance," *Progress In Electromagnetics Research Letters*, Vol. 21, 31–40, 2011.
13. Chin, K.-S. and J.-H. Yeh, "Dual-wideband bandpass filter using shorted stepped-impedance resonators," *IEEE Microw. Wireless Compon. Lett.*, Vol. 19, No. 3, 155–157, 2009.
14. Deng, H-W., B. Liu, Y.-J. Zhao, X.-S. Zhang, and W. Chen, "A stub-loaded triple-mode SIR for novel high selectivity dual-wideband microstrip BPF design," *Progress In Electromagnetics Research Letters*, Vol. 21, 169–176, 2011.
15. Zhang, Z., Y.-C. Jiao, X.-M. Wang, and S.-F. Cao, "Design of compact dual-band bandpass filter using opposite hook-shaped resonator," *IEEE Microw. Wireless Compon. Lett.*, Vol. 21, No. 7, 359–361, 2011.
16. Tang, C.-W. and Y.-K. Hsu, "Design of wide-single/dual-passband filters with comb-loaded resonator," *IET Microw. Antennas Propag.*, Vol. 6, No. 1, 10–16, 2012.
17. Kuo, J.-T., C.-Y. Fan, and S.-C. Tang, "Dual-wideband bandpass filter with extended stopband based on coupled line and coupled three-line resonators," *Progress In Electromagnetics Research*, Vol. 124, 1–15, 2012.
18. Zhou, J. G., W. J. Feng, and W. Q. Che, "Dual-wideband bandpass filter using T-shaped structure based on transversal signal-interaction concepts," *Elecron. Lett.*, Vol. 48, No. 24, 1539–1540, 2012.
19. Xu, J., W. Wu, and C. Miao, "Compact and sharp skirts microstrip dual-mode dual-band bandpass filter using a single quadruple-mode resonator (QMR)," *IEEE Trans. on Microw. Theory and Tech.*, Vol. 61, No. 3, 1104–1113, 2013.
20. Hong, J. S. and M. J. Lancaster, *Microstrip Filter for RF/Microwave Applications*, Wiley, New York, 2001.